Quest for Environmentally-Benign Ligands for Actinide Separations: Thermodynamic, Spectroscopic, and Structural Characterization of U(VI) Complexes with Oxa-Diamide and Related Ligands

Guoxin Tian,[1] Linfeng Rao,[*1] Simon J. Teat,[2] and Guokui Liu[3]

[1]Chemical Sciences Division, Lawrence Berkeley National Laboratory, Berkeley, CA 94720
[2]Advanced Light Source, Lawrence Berkeley National Laboratory, Berkeley, CA 94720
[3]Chemical Sciences and Engineering Division, Argonne National Laboratory, Argonne, IL 60439

Abstract

Complexation of U(VI) with *N,N,N′,N′*-tetramethyl-3-oxa-glutaramide (TMOGA) and *N,N*-dimethyl-3-oxa-glutaramic acid (DMOGA) was studied in comparison with their dicarboxylate analog, oxydiacetic acid (ODA). Thermodynamic parameters, including stability constants, enthalpy and entropy of complexation, were determined by spectrophotometry, potentiometry and calorimetry. Single-crystal X-ray diffractometry, EXAFS spectroscopy, FT-IR absorption and laser-induced luminescence spectroscopy were used to obtain structural information on the U(VI) complexes.

Like ODA, TMOGA and DMOGA form tridentate U(VI) complexes, with three oxygen atoms (the amide, ether and/or carboxylate oxygen) coordinating to the linear UO_2^{2+} cation *via* the equatorial plane. The stability constants, enthalpy and entropy of complexation all decrease in the order ODA > DMOGA > TMOGA, showing that the complexation is entropy driven and the substitution of a carboxylate group with an amide group reduces the strength of complexation

---

[*] Corresponding author. Tel: 510 486 5427. Fax: 510 486 5596. LRao@lbl.gov

1

with U(VI) due to the decrease in the entropy of complexation. The trend in the thermodynamic stability of the complexes correlates very well with the structural and spectroscopic data obtained by single crystal XRD, FT-IR and laser-induced luminescence spectroscopy.

1. Introduction

Alkyl-substituted amides have been studied as extractants for actinide separation because of their potential to make the separation processes more efficient and environmentally-benign. The products of radiolytic and hydrolytic degradation of amides are less detrimental to the separation processes than those of organophosphorus compounds traditionally used in actinide separations (e.g., tributylphosphate). Stripping of actinides from the amide-containing organic solvents is relatively easy. In addition, the amide ligands consist of only C, H, O and N so that they are completely incinerable. As a result, in contrast to the large amounts of liquid and/or solid radioactive wastes generated in traditional organophosphorus-based separation processes, the amount of solid radioactive wastes generated in the amide-based processes could be significantly reduced.

Studies of actinide separation by solvent extraction have recently been conducted with a group of alkyl-substituted oxa-diamides, including tetraoctyl-3-oxa-glutaramide,[1-2] tetraisobutyl-oxa-glutaramide[3] and N,N′-dimethyl-N,N′-dihexyl-3-oxaglutaramide.[4] These ligands form chelate complexes with actinides that can be effectively extracted from nitric acid solutions into organic solvents[1-9] Distribution ratios of actinides under different conditions have been determined in these studies, but the underlying thermodynamic principles governing the complexation of

actinides with oxa-diamides remain unrevealed. Besides, few structural data on these complexes are available. Therefore, we have started systematic studies of three structurally-related ligands, including *N,N,N',N'*-tetramethyl-3-oxa-glutaramide (TMOGA), *N,N*-dimethyl-3-oxa-glutaramic acid (DMOGA) and their dicarboxylate analog - oxydiacetic acid (ODA).[10,11] Thermodynamic parameters (stability constants, enthalpy and entropy of complexation) and structural data (crystal structure, coordination modes and vibration frequency) were obtained to establish a structure – property relationship. The three ligands were selected for this study due to the following reasons: (1) TMOGA is the smallest homologue of tetraalkyl-oxa-glutaramides used as extractants in solvent extraction and is sufficiently soluble in aqueous solutions, so that multiple thermodynamic techniques (potentiometry, spectrophotometry and calorimetry) can be readily applied to this study. (2) DMOGA is the smallest homologue of dialkyl-oxa-glutaramic acids, a major group of hydrolysis and radiolysis products of tetraalkyl-oxa-glutaramides that also form complexes with actinides and affect the separation of actinides.[12] (3) ODA is the dicarboxylate analog of TMOGA and DMOGA, and some thermodynamic and structural data in the literature on the complexes of U(VI) with ODA are available for comparison. As shown in Figure 1, there is a systematic change in structure from TMOGA to DMOGA and ODA, where the amide groups of TMOGA are replaced by one (in DMOGA) and two (in ODA) carboxylate groups. Therefore, the thermodynamic trends obtained for the U(VI) complexes with this series of ligands could provide insight into the energetics and driving force of the complexation (e.g., enthalpy, entropy or both) and help to design effective extractants for actinide separation from nuclear wastes.

In this paper, L^I, L^{II} and L^{III} are used to denote the neutral TMOGA, deprotonated DMOGA (-1 charge) and deprotonated ODA (-2 charge) ligands, respectively.
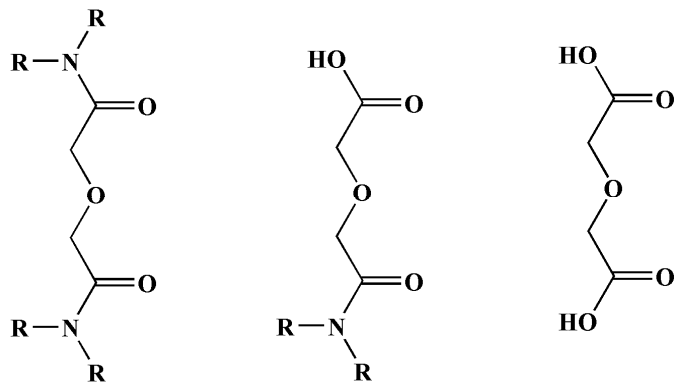
Figure 1. Structurally related ligands (R = methyl): *N,N,N',N'*-Tetramethyl-3-oxa-glutaramide (TMOGA, **L**^{I}, left), *N,N*-Dimethyl-3-oxa-glutaramic acid (DMOGA, H**L**^{II}, center) and oxydiacetic acid (ODA, H$_2$**L**^{III}, right).

2. Experimental Section

2.1 Chemicals

N,N,N',N'-tetramethyl-3-oxa-gutaramide (TMOGA, L^I) was prepared from diglycolyl chloride and dimethyl ammonia (gas) in 1,4-dioxane with vigorous stirring below 5°C, and purified by re-crystallization from water. H-NMR(D$_2$O): 2.7-2.8, double peak (12H, -C(O)N-(CH_3)$_2$); 4.2, single peak (4H, -O-CH_2-C(O)N-(CH$_3$)$_2$). Melting point: 67-68°C. *N,N*-dimethyl-3-oxa-glutaramic acid (DMOGA, HL^{II}) was synthesized from diglycolic anhydride and dimethyl ammonia (gas) in 1,4-dioxane with vigorous stirring below 5°C; and purified by re-crystallization from water. H-NMR(D$_2$O): 2.7-2.8, double peak (6H, -C(O)N-(CH_3)$_2$); 4.1, single peak (2H, HOOC-CH$_2$-O-CH_2-C(O)N-(CH$_3$)$_2$); 4.2, single peak (2H, HOOC-CH_2-O-CH$_2$-C(O)N-(CH$_3$)$_2$). Melting point: 80-82°C. All other chemicals were reagent grade or higher.

Milli-Q water was used in the preparation of all solutions. The stock solution of uranyl perchlorate was prepared by dissolving uranium trioxide (UO$_3$) in perchloric acid (Sigma-Aldrich, Inc.). The concentration of uranium in the stock solution was determined by absorption

spectrophotometry and fluorimetry.[13] The concentration of perchloric acid in the stock solution was determined by Gran's potentiometric method.[14] Stock solutions of L^I and L^{II} were prepared by dissolving appropriate amounts of the ligands in water. The concentration of L^I was directly calculated from the weight (M.W. = 188.23) while the concentration of L^{II} was determined potentiometrically with a standard carbonate-free NaOH solution. The ionic strength of all working solutions used in potentiometry, calorimetry and spectrophotometry was adjusted to 1.0 M at 25°C by adding appropriate amounts of sodium perchlorate or nitrate as the background electrolyte. The ionic medium of sodium nitrate was used exclusively in the studies of U(VI)/L^I complexation, because the U(VI)/L^I complex was found to precipitate in the sodium perchlorate media.

2.2 Thermodynamic Measurements

Potentiometry. The protonation constant of L^{II} and the stability constants of the U(VI)/L^{II} complexes were determined by potentiometric titrations at 25°C. Detailed description of the titration setup and the procedure for calibrating the electrode to measure the hydrogen ion concentration have been provided elsewhere.[15]

Multiple titrations were conducted with solutions of different concentrations (C_L, C_H and C_U). Fifty to seventy data points were collected in each titration. The protonation constant of L^{II} and the formation constants of U(VI)/L^{II} complexes were calculated with the program Hyperquad 2000.[16]

Spectrophotometry. Spectrophotometric titrations were carried out with a Cary 5G spectrophotometer from 380 to 480 nm (0.2 nm interval) to determine the stability constants of U(VI) complexes with L^I, L^{II} and L^{III}. The stability constants were calculated by non-linear regression using Hyperquad2000.[16]

Calorimetry. An isothermal microcalorimeter (ITC 4200, Calorimetry Sciences Corp.) was used to determine the enthalpies of the protonation of L^{II} and the complexation of U(VI) with L^{I} and L^{II}. Information on the microcalorimeter, its calibration and the titration procedure has been provided previously.[17] Multiple titrations using different concentrations of the reagents (C_L, C_H and C_U) were performed to reduce the uncertainty of results. The reaction heats measured by microcalorimetry were used, in conjunction with the equilibrium constants obtained by potentiometry and/or spectrophotometry, to calculate the enthalpy of protonation or complexation with the computer program Letagrop.[18]

2.3 Determination of the Structures of U(VI) Complexes

Single crystal X-ray diffractometry. Pale yellow crystals of 1:2 U(VI) complexes, $UO_2(L^{I})_2(ClO_4)_2$, $UO_2(L^{II})_2(H_2O)(NaClO_4)_2$ and $Na_2UO_2(L^{III})_2(H_2O)$ were obtained by slow evaporation from aqueous $UO_2(ClO_4)_2$ solutions containing the three ligands, respectively. Representative crystals of each compound were chosen, $UO_2(L^{I})_2(ClO_4)_2$ was sealed in glass capillary tubes, while the other compounds were picked up on Kapton mounts, before being placed on the goniometer. Diffraction data for $UO_2(L^{I})_2(ClO_4)_2$ were collected on a Bruker AXS APEX diffractometer with graphite monochromated Mo-Kα radiation. For $UO_2(L^{II})_2(H_2O)(NaClO_4)_2$ and $Na_2UO_2(L^{III})_2(H_2O)$, the diffraction data were collected on a Bruker AXS APEX II diffractometer using a silicon (111) monochromator at 0.77490 Å on Beamline 11.3.1 of the Advanced Light Source (ALS). The structure solution and refinement were performed using the SHELXTL crystallographic software package of the Brüker Analytical X-ray System.[19] Details of the crystallographic data are provided in Table 1.

Table 1. Crystallographic data for $UO_2(\mathbf{L^I})_2(ClO_4)_2$, $UO_2(\mathbf{L^{II}})_2(H_2O)(NaClO_4)_2$ and $Na_2UO_2(\mathbf{L^{III}})_2(H_2O)$ complexes.

	$UO_2(\mathbf{L^I})_2(ClO_4)_2$	$UO_2(\mathbf{L^{II}})_2(H_2O)(NaClO_4)_2$	$Na_2UO_2(\mathbf{L^{III}})_2(H_2O)$
Empirical formula	$C_{16}H_{32}Cl_2N_4O_{16}U$	$C_{12}H_{22}Cl_2N_2Na_2O_{19.25}U$	$C_8H_{16}Na_2O_{16}U$
Formula weight	845.39	857.23	652.22
T (K)	160(2)	90(2)	150(2)
Wavelength (Å)	Mo-Kα, 0.71073	synchrotron, 0.77490	synchrotron, 0.77490
Crystal system	monoclinic	triclinic	monoclinic
Space group	$P2(1)/n$	Ccca	$C2/m$
a (Å)	5.7846(6)	44.659(11)	12.188(5)
b (Å)	10.8609(11)	10.8460(19)	7.023(3)
c (Å)	23.049(2)	11.336(3)	10.037(4)
α (deg)	90	90	90
β (deg)	94.728(2)	90	98.163(5)
γ (deg)	90	90	90
V (Å^3)	1443.2(3)	5491(2)	850.4(6)
Z	2	8	2
$\rho_{calculated}$ (g·cm^{-3})	1.945	2.074	2.547
μ (mm^{-1})	5.884	3.557	5.281
$F(000)$	820	3280	612
Crystal size (mm^3)	$0.15 \times 0.11 \times 0.09$	$0.10 \times 0.10 \times 0.01$	$0.04 \times 0.03 \times 0.02$
θ range for data collection	2.07 to 26.47°	3.77 to 33.72°	3.68 to 29.10°
Limiting indices	$-7 < h < 7$	$-60 < h < 63$	$-15 < h < 15$
	$-13 < k < 13$	$-15 < k < 15$	$-8 < k < 8$
	$-18 < l < 28$	$-16 < l < 16$	$-12 < l < 12$
No. of reflections collected	8199	34493	4382
Independent reflections	2933 ($R_{int} = 0.0237$)	4190 ($R_{int} = 0.0463$)	932 ($R_{int} = 0.0640$)
Completeness to θ	26.47°, 98.2 %	30.00°, 99.7 %	29.10°, 97.0 %
Refinement method	full-matrix least-squares on F^2	full-matrix least-squares on F^2	full-matrix least-squares on F^2
Data / restraints / parameters	2933 / 0 / 178	4190 / 63 / 179	932 / 54 / 79
Goodness-of-fit on F^2	1.049	1.101	1.114
Final R indices [$F^2 > 2\sigma(I)$]	$R1 = 0.0290$	$R1 = 0.0406$	$R1 = 0.0241$
	$wR2 = 0.0686$	$wR2 = 0.1029$	$wR2 = 0.0620$
R indices (all data)	$R1 = 0.0445$	$R1 = 0.0651$	$R1 = 0.0241$
	$wR2 = 0.0742$	$wR2 = 0.1144$	$wR2 = 0.0620$
Largest diff. peak and hole	1.300 and -0.764 e Å^{-3}	2.006 and -2.424 e Å^{-3}	1.296 and -1.681 e Å^{-3}

Extended X-ray absorption fine structure spectroscopy (EXAFS). To compare the structures of the U(VI) complexes in solution and in the crystal, uranium L_{III}-edge EXAFS spectra of two solution samples of U(VI)/L^{II} complexes and one solid sample of the 1:2 U(VI)/L^{II} complex were collected at the Stanford Synchrotron Radiation Laboratory (SSRL) on wiggler beam line 11-2. The conditions of the two solution samples were such that the dominant species in the solutions are the 1:1 complex, $UO_2(L^{II})^+$, and 1:2 complex, $UO_2(L^{II})_2$, respectively. Approximately 1 mL of the solution was sealed in a polyethylene tube (5 mm i.d.). The solid sample was prepared by mixing appropriate amounts of the compound with boron nitride and loading the mixture to aluminum holders with a rectangular opening of 20 mm (W) $\times$ 2 mm (H). The polyethylene tubes or aluminum holders were mounted on an aluminum sample positioner with Scotch tape for the experiments. Data were collected up to $k_{max} \sim 13.5$ Å^{-1} in both transmission and fluorescence modes. Three to six scans were performed for each sample. Energy calibrations were based on assigning the first inflection point of absorption edge for uranium dioxide to 17166 eV. The EXAFS data were analyzed with the program WinXAS,[20] using parameterized phase and amplitude functions generated by FEFF8.[21] Single scattering interactions of U=O_{axial} (axial oxygen) and U-O_{eq} (equatorial oxygen) were included.

2.4 Spectroscopic Characterization

FT-IR. Infra-red absorption spectra of solid samples of $UO_2(L^{I})_2(ClO_4)_2$, $UO_2(L^{II})_2(H_2O)(NaClO_4)_2$ and $Na_2UO_2(L^{III})_2(H_2O)$ were collected with KBr plates on a Mattson Sirius 100 FT-IR in a range from 500 to 4000 cm^{-1} with 2 cm^{-1} resolution.

Laser-induced luminescence spectroscopy. Laser-induced luminescence spectra of solid samples of $UO_2(L^{I})_2(ClO_4)_2$, $UO_2(L^{II})_2(H_2O)(NaClO_4)_2$ and $Na_2UO_2(L^{III})_2(H_2O)$ were collected using an Ar$^+$ ion laser with wavelength at 458 nm. The samples were placed in a helium cryostat

for low temperature measurements. The luminescence was dispersed by a monochromator mounted with a cooled photomultiplier and recorded through a lock-in amplifier.

3. Results and Discussion

3.1 Thermodynamic Parameters and Trends

Protonation constant and enthalpy of DMOGA (HL^{II}). The protonation constant of L^{II} was calculated to be log K = 3.49 (at I = 1.0 M and t = 25°C) from the data obtained by potentiometry. Compared with other mono-carboxylic acids, DMOGA is a stronger acid than simple alkyl carboxylic acids such as acetic (log K = 4.57) and propanoic acids (log K = 4.67), but is very similar in strength to alkoxycarboxylic acids such as methoxyacetic acid (log K = 3.4) and ethoxyacetic acid (log K = 3.51)[22] - all having an ether oxygen. This comparison suggests that, due to the electron-withdrawing ability of the ether oxygen, the effective negative charge on the carboxylate group in L^{II} is smaller than that in alkylcarboxylates. In addition, the distant amide group in L^{II} seems to have little effect on the acidity of the carboxylate group. The enthalpy of protonation of L^{II} determined by calorimetry is small and positive (0.83 kJ/M), typical of monocarboxylic acids.

Stability constants of U(VI) complexes with TMOGA (L^{I}), DMOGA (HL^{II}) and ODA (H$_2$L^{III}). Figure 2 shows representative sets of absorption spectra for the titration of U(VI) with L^{I}, L^{II} and L^{III}. In all titrations, three significant changes in the spectra are observed as the concentration of the ligands increases: 1) the positions of the absorption bands of U(VI) are red-shifted; 2) the intensities of the bands increase; 3) the intensities of the branches from 440 to 480 nm increase more significantly than other branches, indicating that the relative intensities of the vibronic branches in the U(VI) complexes are quite different from those in free UO$_2^{2+}$. Analysis with the Hyperquad program indicates that the spectral changes can be described by successive

formation of 1:1 and 1:2 U(VI)/ligand complexes. Using the HyperQuad program, the stability

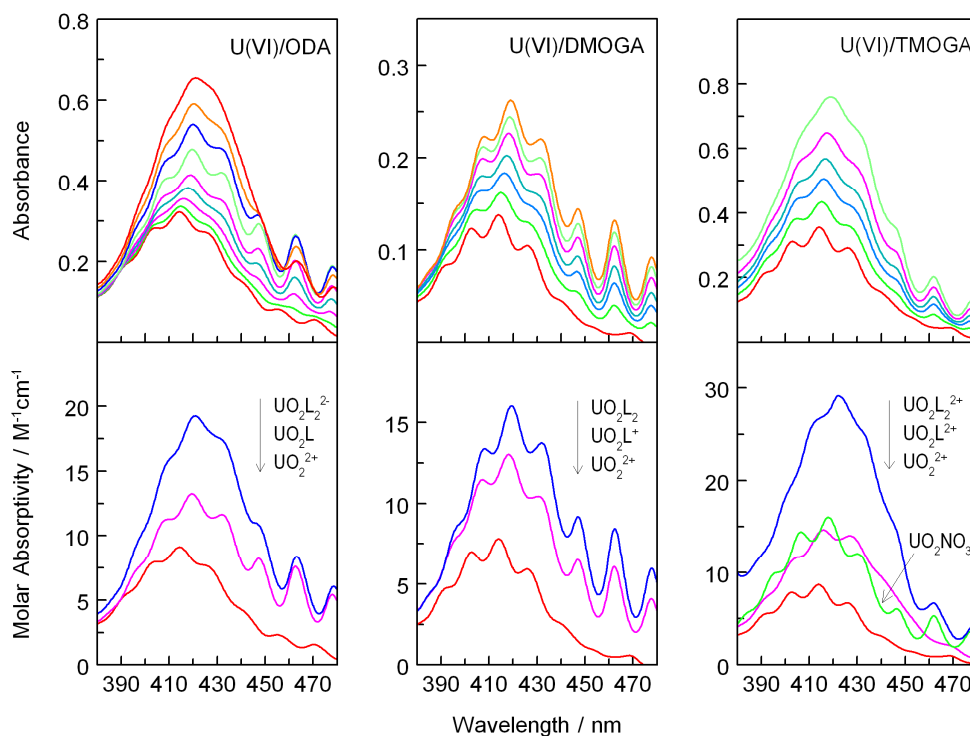constants (Table 2) and molar absorptivity (Figure 2) of the complexes were calculated.

Figure 2. Spectrophotometric titrations of the complexation of U(VI) with TMOGA, DMOGA and ODA (t = 25°C, I = 1.0 M NaNO$_3$ for the TMOGA system and 1.0 M NaClO$_4$ for the DMOGA and ODA systems, initial cuvette solution 2.50 ml). Upper figures - absorption spectra normalized to account for dilution due to volume increase along the titration; lower figures – calculated molar absorptivity of U(VI) species. Right - U(VI)/TMOGA: C_H = 0.0500 M, C_U = 0.0400 M. Titrant: C_{TMOGA} = 0.400 M. Center - U(VI)/DMOGA: C_H = 0.0212 M, C_U = 0.0177 M. Titrant: C_H = 0.01915 M, C_{DMOGA} = 0.2192 M. Left - U(VI)/ODA: C_H = 0.044 M, C_U = 0.0354 M. Titrant: 0.250 M Na$_2$ODA.

As shown in Table 2, the stability constants of the U(VI)/L^{II} complexes obtained by

spectrophotometry and potentiometry in this work are in excellent agreement. For the U(VI)/L^{III}

complexes, the values of logβ_1 by spectrophotometry in this work and potentiometry in the

literature[15] agree very well (4.91 and 5.01), but the values of log β_2 differ significantly (7.39 and

7.64). The disagreement in $\log\beta_2$ probably results from the fact that the model for the potentiometric titrations[15] includes a protonated 1:2 U(VI)/L^{III} complex (MHL_2) while the model for the spectrophotometric titrations does not. The difference in the absorption spectra between the ML_2 and MHL_2 species might be too subtle to distinguish in spectrophotometry.

Table 2. Complexation of UO_2^{2+} with TMOGA, DMOGA and ODA ($t = 25^{\circ}C$). Methods: pot – potentiometry, sp – spectrophotometry, cal – calorimetry. Reference: p.w. - present work.

Ligand	Reaction	I	Method	$\log\beta$	ΔH kJ·mol^{-1}	ΔS J·K^{-1}·mol^{-1}	Ref.
TMOGA	$UO_2^{2+} + L = UO_2L^{2+}$	1.0 M NaNO$_3$	sp, cal	1.71 ± 0.03	7.47 ± 0.27	58 ± 1	p.w.
($\mathbf{L^I}$)	$UO_2^{2+} + 2L = UO_2L_2^{2+}$			2.94 ± 0.01	19.6 ± 0.5	122 ± 1	
DMOGA ($H\mathbf{L^{II}}$)	$UO_2^{2+} + L^- = UO_2L^+$	1.0 M NaClO$_4$	pot, cal sp	3.81 ± 0.02 3.90 ± 0.02	15.0 ± 0.1	124 ± 1	p.w.
	$UO_2^{2+} + 2L^- = UO_2L_2(aq)$		pot, cal sp	5.88 ± 0.02 5.88 ± 0.02	21.6 ± 0.2	185 ± 1	
ODA ($H_2\mathbf{L^{III}}$)	$UO_2^{2+} + L^{2-} = UO_2L(aq)$	1.0 M NaClO$_4$	pot, cal sp	5.01 ± 0.04 4.91 ± 0.01	16.4 ± 0.2	152 ± 1	[15] p.w.
	$UO_2^{2+} + 2L^{2-} = UO_2L_2^{2-}$		pot, cal sp	7.64 ± 0.07 7.39 ± 0.03	23.8 ± 0.1	227 ± 2	[15] p.w.

Because the spectrophotometric titrations of U(VI)/L^I were performed in 1 M NaNO$_3$, the stability constant of the U(VI)/nitrate complex, $UO_2(NO_3)^+$, must be known so that corrections can be made to account for the complexation of U(VI) with nitrate. A separate set of spectrophotometric titrations with U(VI)/nitrate were carried out and the values of $\log\beta_1$ for $UO_2(NO_3)^+$ was determined to be $-(0.62 \pm 0.04)$ at $I = 1$ M and $t = 25^{\circ}C$.[23] This value, within the range that the scattered literature values span (from -0.77 to -0.3 at $I = 1 - 2$ M and $t = 20 - 25^{\circ}C$),[24] was accordingly used in the analysis of the titration data for U(VI)/L^I. As the lower-right plot of Figure 2 shows, the titration of U(VI)/TMOGA is best represented by the formation of two U(VI)/L^I complexes and $UO_2(NO_3)^+$.

Enthalpy of complexation. Figure 3 shows representative calorimetric titrations of U(VI)/L$^{\text{I}}$ and U(VI)/L$^{\text{II}}$ complexation. The stepwise reaction heat, $Q_{\text{r,i}}$, as well as the distribution of U(VI) species, is shown as a function of the titrant volume added into the cell. Negative values of $Q_{\text{r,i}}$ indicate that the complexation reactions are endothermic. From the results of multiple titrations with different concentrations of U(VI) and acidity, the enthalpies of complexation for the 1:1 and 1:2 U(VI) complexes with L$^{\text{I}}$ and L$^{\text{II}}$ were calculated and summarized in Table 2. A value of ΔH (3.9 $\pm$ 0.5 kJ/M) for the reaction $UO_2^{2+} + NO_3^- = UO_2(NO_3)^+$, determined in a previous study,[23] was included in the calculation for the U(VI)/L$^{\text{I}}$ complexes to correct for the formation of $UO_2(NO_3)^+$ in the calorimetric titrations.
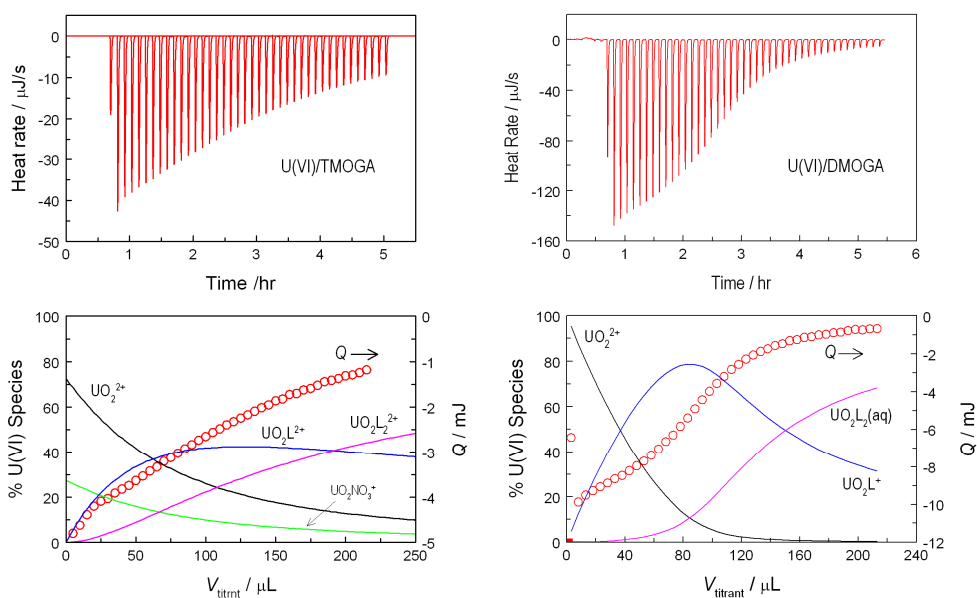
Figure 3. Calorimetric titration of the complexation of U(VI)-TMOGA and U(VI)/DMOGA systems (t = 25$^{\text{o}}$C). Left – U(VI)/TMOGA, I = 1.0 M NaNO$_3$. Initial cup solution (0.900 ml): C_{H} = 14.0 mM, C_{U} = 11.1 mM. Titrant: C_{TMOGA} = 0.400 M. Right - U(VI)/DMOGA, I = 1.0 M NaClO$_4$. Initial cup solution (0.900 ml): C_{H} = 12.22 mM, C_{U} = 9.833 mM. Titrant: C_{H} = 0.0109 M, C_{DMOGA} = 0.2282 M. For both systems, top - thermogram; bottom - stepwise heat (○, left y-axis) and speciation of U(VI) (lines, right y-axis) vs. the volume of titrant.

Thermodynamic trends: amide group *vs*. carboxylate group. Data from this work show that, from TMOGA (two –C(O)N(CH$_3$)$_2$ groups) to DMOGA (one –COOH and one –C(O)N(CH$_3$)$_2$ group) and ODA (with two -COOH groups), the enthalpy of complexation (ΔH) becomes more endothermic and less favorable to the complexation while the entropy of complexation (ΔS) becomes larger and more favorable to the complexation (Table 2). Such trends imply that the carboxylate group (–COO$^-$) is more hydrated than the carbonyl group (–C=O) in the amide moiety. When forming complexes with UO$_2^{2+}$, more energy is required to dehydrate the carboxylate group and more water molecules are released from the hydration sphere of the carboxylate group than the amide group, resulting in more endothermic enthalpy and larger entropy of complexation from TMOGA to DMOGA, and further to ODA. In addition, another mechanism as follows could contribute to the observed trend in the entropy. Because the positive charge on the U(VI) complexes decrease in the order TMOGA > DMOGA > ODA, the solvation sphere of the U(VI) complex probably becomes less ordered from TMOGA to DMOGA and ODA, resulting in larger entropy gain in the complexation along the series. In summary, the enthalpy and the entropy of complexation both increase in the order: U(VI)/TMOGA < U(VI)/DMOGA < U(VI)/ODA. The complexation of U(VI) with all three ligands is entropy driven. Consequently, TMOGA and DMOGA are weaker ligands in aqueous solutions than ODA due to a less favorable entropy effect.

3.2 Structure and Coordination Modes

Crystal structures of UO$_2$(L^I)$_2$(ClO$_4$)$_2$, UO$_2$(L^{II})$_2$(H$_2$O)(NaClO$_4$) and Na$_2$UO$_2$(L^{III})$_2$(H$_2$O). Selected bond lengths and the O=U=O bond angle are given in Table 3.

UO$_2$(L^I)$_2$(ClO$_4$)$_2$. The perchlorate salt of the 1:2 U(VI)/L^I complex, UO$_2$(L^I)$_2$(ClO$_4$)$_2$, crystallized in a monoclinic space group, *P*2(1)/n. The axial O=U=O moiety is linear (180°

angle) and symmetrical (U=O_{axial} bond length = 1.752(3) Å). The two L^I ligands are coplanar and each coordinates to UO_2^{2+} with three oxygen atoms (two from the amide groups and one ether oxygen) in the equatorial plane. The U-O_{ether} bond length is 2.614(3) Å, longer than those of the two U–O_{amide} bonds (2.416(4) Å and 2.421(3) Å). The molecule is centrosymmetric and the uranium atom is at the inversion center as shown in Figure 4a.

$UO_2(L^{II})_2(H_2O)(NaClO_4)_2$. The 1:2 U(VI)/$L^{II}$ complex crystallized as a mixed salt, $UO_2(L^{II})_2(H_2O)(NaClO_4)_2$, in a triclinic space group, *C*cca. The axial O=U=O moiety is slightly bent (179.2°) with R(U=O_{axial}) = 1.758(5) Å. Each of the two L^{II} ligands coordinates to UO_2^{2+} with three oxygen atoms (one from the carboxylate group, one from the amide groups and one ether oxygen) in the equatorial plane. The U-O_{ether} bond length is 2.569 Å, longer than those of the U–$O_{carboxylate}$ and U–O_{amide} bonds (2.429 Å and 2.439 - 2.440 Å) (Figure 4b).

$Na_2UO_2(L^{III})_2(H_2O)$. The 1:2 U(VI)/$L^{III}$ complex crystallized as a mixed salt, $Na_2UO_2(L^{III})_2(H_2O)$, in a monoclinic space group, *C*2/m. The axial O=U=O moiety is perfectly linear (180° angle) and symmetrical (U=O_{axial} bond length = 1.764(6) Å). The two L^{III} ligands are coplanar and each coordinates to UO_2^{2+} with three oxygen atoms (two from the carboxylate groups and one ether oxygen) in the equatorial plane. The U-O_{ether} bond length is 2.666 Å, longer than those of the two U–$O_{carboxylate}$ bonds (2.379 Å and 2.418 Å). The molecule is centrosymmetric and the uranium atom is at the inversion center as shown in Figure 4c. This structure is very similar to that of a 1:2 U(VI)/ODA complex in a mixed organic ammonium salt, $[C_2H_5NH_2(CH_2)_2NH_2C_2H_5][UO_2(L^{III})_2]$, reported in the literature.[25]
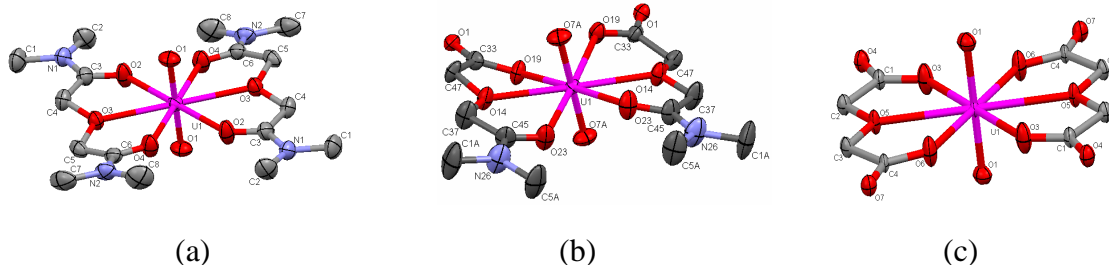
Figure 4. Structures of three U(VI) complexes in crystals (50% probability ellipsoids). (a) $UO_2(\mathbf{L^I})_2(ClO_4)_2$; (b) $UO_2(\mathbf{L^{II}})_2(H_2O)(NaClO_4)_2$; (c) $Na_2UO_2(\mathbf{L^{III}})_2(H_2O)$. Hydrogen, sodium, water and perchlorate moieties are not shown for clarity.

Table 3. Selected bond lengths (Å) and bond angle (deg) in $UO_2(\mathbf{L^I})_2(ClO_4)_2$, $UO_2(\mathbf{L^{II}})_2(H_2O)(NaClO_4)_2$ and $Na_2UO_2(\mathbf{L^{III}})_2(H_2O)$.

	$UO_2(\mathbf{L^I})_2(ClO_4)_2$	$UO_2(\mathbf{L^{II}})_2(H_2O)(NaClO_4)_2$	$Na_2UO_2(\mathbf{L^{III}})_2(H_2O)$
U=O$_{axial}$	1.752 (3), 1.752 (3)	1.758 (5), 1.758 (5)	1.764 (6), 1.764 (5)
U-O$_{amide}$	2.416 (4), 2.416 (4)	2.439 (5), 2.440 (5)	
	2.421 (3), 2.421 (3)		
U-O$_{carboxylate}$		2.429 (5), 2.429 (5)	2.379 (6), 2.379 (6)
			2.418 (6), 2.418 (6)
U-O$_{ether}$	2.614 (3), 2.614 (3)	2.569 (5), 2.569 (5)	2.666 (5), 2.666 (5)
∠O=U=O	180.00 (18)	179.2 (3)	180.0

Comparison between the structures in solution and solids. The structures of the 1:1 U(VI)/L^{II} complexes in solution and the 1:2 U(VI)/L^{II} complexes in solution and solids were obtained by fitting the EXAFS data. The k^3-weighted U(VI) EXAFS spectra and corresponding Fourier Transform (FT) magnitude (phase shift not corrected) are shown in Figure 5.

The FT magnitudes of all three samples (Solutions 1 and 2, and the solid) have a predominant peak at low R (~ 1.3 Å before phase shift correction) that can be well fitted with two

U-O scattering paths at 1.77-1.78 Å, corresponding to the two "axial" oxygen atoms in the UO_2^{2+} cation. The smaller peak at longer distances (~ 1.8-1.9 Å before phase shift) is also similar for all three samples, but is slightly broadened from Solution 1 to Solution 2 and the solid sample. This feature can be fitted with two coordination shells, one at 2.38 – 2.41 Å and the other at 2.54 to 2.59 Å, containing oxygen atoms equatorially coordinated to uranium. The best fit indicates that the coordination shell at 2.38 – 2.41 Å contains four oxygen atoms for all three samples. However, the coordination shell at 2.54 – 2.59 Å contains one oxygen atom for Solution 1 but two oxygen atoms for Solution 2 and the solid sample.
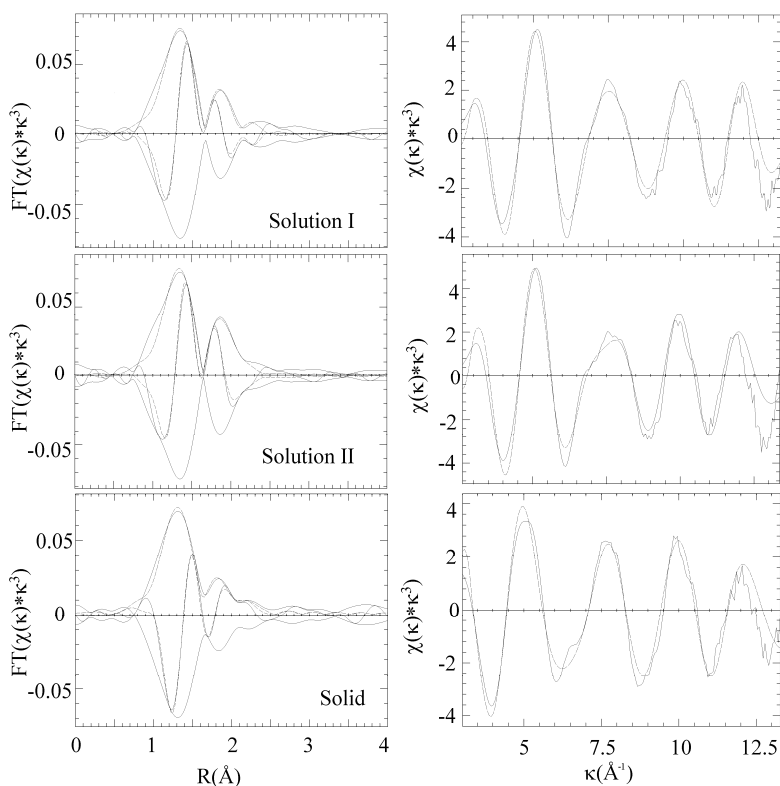
Figure 5. Experimental (dashed lines) and fitted (dotted lines) uranium L_{III}-edge EXAFS spectra (right) and associated Fourier transform magnitude (left).

Based on the structure of the $UO_2(L^{II})_2$ complex in the $UO_2(\mathbf{L^{II}})_2(H_2O)(NaClO_4)_2$ crystal (Figure 4b), it is reasonable to assign the coordination shells of the complexes in the two solution

samples as follows. (1) The 1:1 U(VI)/L^{II} complex in solution contains one tridentate L^{II} and two water molecules. The four oxygen atoms at 2.38 Å are from the carboxylate and amide groups of the L^{II} ligand and two water molecules. The oxygen atom from the ether group of the L^{II} ligand is at 2.57 Å. (2) The 1:2 U(VI)/L^{II} complex in solution contains two tridentate L^{II} ligands. The four oxygen atoms at 2.39 Å are from the carboxylate and amide groups of two L^{II} ligands. Two oxygen atoms from the ether groups of the two L^{II} ligands are at 2.54 Å. The best-fit parameters from EXAFS, the assignments of coordination modes and the proposed structures of the U(VI)/L^{II} complexes in solution are shown in Table 4.

Table 4. Best-fit parameters for U L$_{III}$- edge EXAFS

Sample	Shell	R(Å)	CN	σ^2(Å^2)	ΔE^0(eV)	Proposed Structure
Solution 1: UO$_2$(**L^{II}**)$^+$ (79%) C_U = 0.03 M, C_L = 0.03 M, pH = 5	U-O$_{ax}$	1.77	2.0	0.002	9.8	
	U-O$_{eq1}$	2.38	4.1	0.008	9.8	
	U-O$_{eq2}$	2.57	1.0	0.002	9.8	
Solution 2: UO$_2$(**L^{II}**)$_2$ (90%) C_U = 0.03 M, C_L = 0.15 M, pH = 5	U-O$_{ax}$	1.77	2.0	0.002	10.7	
	U-O$_{eq1}$	2.39	3.9	0.007	10.7	
	U-O$_{eq2}$	2.54	1.9	0.005	10.7	
Solid sample: UO$_2$(**L^{II}**)$_2$ (values in parentheses are cystallographic data)	U-O$_{ax}$	1.76 (1.758)	2.0 (2)	0.002	7.6	(Figure 4b)
	U-O$_{eq1}$	2.41 (2.429) (2.429) (2.439) (2.440)	3.8 (4)	0.008	7.6	
	U-O$_{eq2}$	2.59 (2.569)	1.8 (2)	0.004	7.6	

It is interesting to notice that the proposed structure of the 1:2 U(VI)/L^{II} complex in solution is different from that in the crystal in terms of the arrangement of the two L^{II} ligands in the equatorial coordination plane. The proposed structure in solution contains the two L^{II} ligands in a "staggered" manner, i.e., the two carboxylate groups (or the two amide groups) are "diagonal" to each other in the equatorial coordination plane. In contrast, the two carboxylate groups (or the two amide groups) in the UO$_2$(L^{II})$_2$(H$_2$O)(NaClO$_4$)$_2$ are actually "head-on" to each other (Figure 4b). The "head-on" arrangement in the solids is stable due to the interactions with adjacent sodium ions in the crystal lattice (not shown in Figure 4b), but may not be the most probable structure in solution because the constraints set by the strong interactions in the crystal lattice are absent in solution. Instead, surrounded by water molecules, the "staggered" arrangement is likely to be the structure with the lowest energy, though the EXAFS data provide only the information on radial distribution and do not suffice such proposal.

3.3 Correlation between Thermodynamic Trends and Structural Data.

Stretching frequencies of the ligand C=O and C-O-C bonds. The FT-IR spectra (500 to 2000 cm^{-1}) of the three ligands and their complexes with U(VI) contain many features associated with the vibrational modes of the carbonyl (C=O) and ether oxygen (C-O-C) bonds (Figure 6). Selected stretching frequencies of these bonds in the free ligands and the complexes are summarized in Table 5. In general, for all three ligands, the stretching frequencies of the C=O and C-O-C bonds are red-shifted, indicating the weakening of these bonds due to the complexation with UO$_2^{2+}$. The magnitude of the red-shift, $|\Delta v|$ in cm^{-1}, should be a good measure of the complexation strength of the complexes. As the data in Table 5 show, the values of $|\Delta v|$ for the C=O and C-O-C bonds all follow the order: L^I < L^{II} < L^{III}. This is consistent with the thermodynamic trend in the stability of the complexes shown in Table 2: the stability

constants of both the 1:1 and 1:2 complexes (log β_1 and log β_2) follow the order: $U(VI)/L^I <$ $U(VI)/L^{II} < U(VI)/L^{III}$.
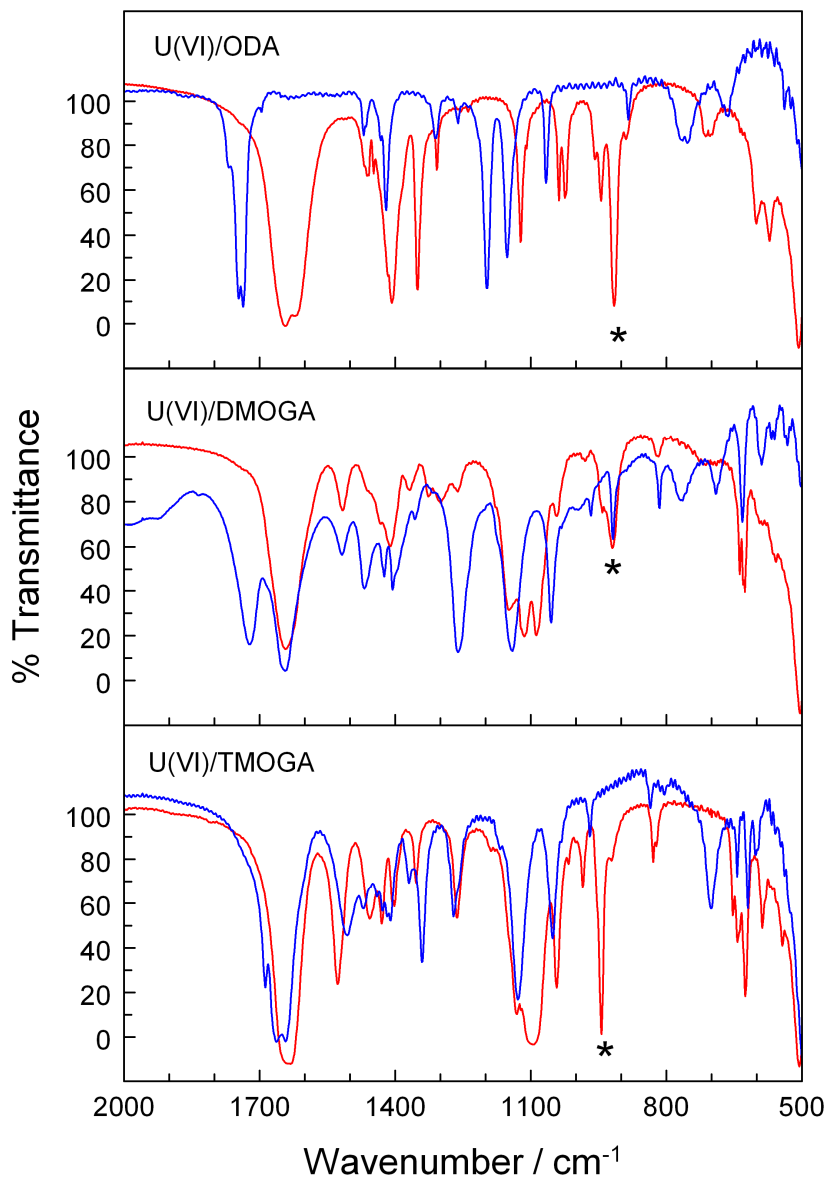

Figure 6. IR spectra of the three ligands (TMOGA, DMOGA and ODA) and their 1:2 complexes with UO_2^{2+}. Blue lines – ligands; Red lines – complexes in $UO_2(\mathbf{L^I})_2(ClO_4)_2$, $UO_2(\mathbf{L^{II}})_2(H_2O)(NaClO_4)_2$ and $Na_2UO_2(\mathbf{L^{III}})_2(H_2O)$. * - Absorption bands assigned to the asymmetric stretching mode of UO_2^{2+}.

Table 5. FT-IR data: perturbation of the stretching frequencies of the carbonyl and ether oxygen bonds in the three ligands upon complexation with U(VI).

	ν_{symm}, cm^{-1} (C=O)			ν_{asymm}, cm^{-1} (-O-)			ν_{symm}, cm^{-1} (-O-)		
	free ligand	complex	$\Delta\nu$	free ligand	complex	$\Delta\nu$	Free ligand	complex	$\Delta\nu$
TMOGA (**L^{I}**)	1688	1646	-42	1129	1104	-25	1052	1043	-9
DMOGA (H**L^{II}**)	1733	1657	-76	1142	1116	-26	1055	1045	-10
ODA (H$_2$**L^{III}**)	1737	1647	-90	1152	1122	-30	1067	1038	-29
	1746		-99						

O=U=O bond length. The bond length as well as the symmetric and asymmetric stretching frequencies of the axial O=U=O bonds are also sensitive to the equatorial coordination environment. Complexation with ligands *via* equatorial plane usually weakens the axial O=U=O bond, which could lead to bond elongation. The degree of O=U=O bond lengthening is in turn a measure of the complexation strength of the complex. Crystal structural data from this work show that, indeed, the bond length ($R_{U=O}$) in the three complexes follows the order: UO$_2$(L^{I})$_2$ < UO$_2$(L^{II})$_2$ < UO$_2$(L^{III})$_2$ (Table 6), consistent with the thermodynamic trend in the stability of the complexes.

Table 6. Axial U=O bond length (R), stretching frequency (ν) and the luminescence emitting state energy level (ΔE) of the three U(VI) complexes.

	R (U=O$_{axial}$), Å (XRD)	ν_{symm}, cm^{-1} (luminescence)	ν_{asymm}, cm^{-1} (FT-IR)	ΔE, cm^{-1} (luminescence)
UO$_2$(**L^{I}**)$_2^{2+}$	1.752(3)	860	944	20198
UO$_2$(**L^{II}**)$_2$	1.758(5)	856	920	20137
UO$_2$(**L^{III}**)$_2^{2-}$	1.764(6)	828	916	20026

Symmetric stretching frequencies of O=U=O. The stretching frequencies of the O=U=O bond are expected to correlate with the strength of equatorial ligand coordination.[26,27] In this work, the symmetric O=U=O stretching frequencies were obtained by laser-induced luminescence spectroscopy. The emission spectra for the three complexes are shown in Figure 7. The charge transfer vibronic transitions of U(VI) consist of multi-phonon progressions caused by the O=U=O symmetric stretch mode.[28,29] From these features, the symmetric stretching frequencies of the O=U=O bond (ν_{symm}) in the complexes are calculated to be 860, 856 and 828 cm^{-1} for the UO$_2$(L^I)$_2$, UO$_2$(L^{II})$_2$ and UO$_2$(L^{III})$_2$ complexes, respectively. These frequencies refer to the ground state configuration and the order of ν_{symm} is consistent with the thermodynamic trend in the stability of the complexes (Table 2), as well as the trend in the O=U=O bond length (Table 6).
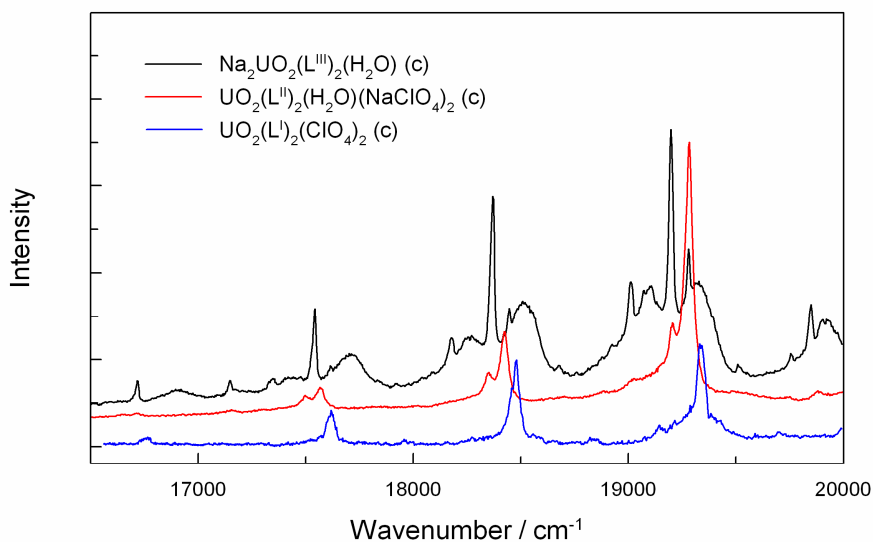

Figure 7. Laser-induced luminescence emission spectra of three U(VI) compounds, UO$_2$(**L^I**)$_2$(ClO$_4$)$_2$, UO$_2$(**L^{II}**)$_2$(H$_2$O)(NaClO$_4$)$_2$ and Na$_2$UO$_2$(**L^{III}**)$_2$(H$_2$O). Excitation wavelength = 458 nm, T = 77 K.

In contrast to the luminescence spectra, the UV absorption spectra can provide symmetric stretching frequencies of U(VI) in the first excited state. From the progressing peaks in the absorption spectra at 25°C (Figure 2), values of ν_{symm} are estimated to be 730, 710 and 700 cm^{-1}, respectively for the $UO_2(L^{I})_2$, $UO_2(L^{II})_2$ and $UO_2(L^{III})_2$ complexes. Not surprisingly, all ν_{symm} values for the excited state are lower than those for the ground state, since the O=U=O bond in the excited state is expected to expand and the stretching frequency is reduced accordingly.

Asymmetric stretching frequencies of O=U=O. For UO_2^{2+} in crystals, the O=U=O asymmetric stretching frequency may also be observable in the luminescence spectra as sidelines accompanying the progressing lines of the symmetric mode. As shown in Figure 7, the features for the asymmetric mode are clearly seen in the spectrum for the $UO_2(\mathbf{L^{II}})_2$ complex and the frequency is calculated to be 929 cm^{-1}. However, the asymmetric stretching frequencies for the other two complexes, $UO_2(\mathbf{L^{I}})_2$ and $UO_2(\mathbf{L^{III}})_2$, are difficult to quantify by the luminescence spectra, probably because the existence of defect sites or impurity phases in the samples obscured the features of asymmetric stretching mode.

Measurements of the asymmetric stretching frequencies of the O=U=O bond in all three complexes were achieved by FT-IR (Figure 6). Data in Table 6 indicate that ν_{asymm} decreases in the order: $UO_2(L^{I})_2$ (944 cm^{-1}), $UO_2(L^{II})_2$ (920 cm^{-1}), $UO_2(L^{III})_2$) (916 cm^{-1}). Again, this trend agrees with the thermodynamic trend in the stability of the complexes as well as the trends in the bond length and symmetric stretching frequencies of UO_2^{2+} in the three complexes. It is noted that the value of ν_{asymm} for $UO_2(L^{II})_2$ obtained by FT-IR (920 cm^{-1}) is 9 cm^{-1} lower than that by laser luminescence (929 cm^{-1}). Such small difference is not surprising since the two measurements were performed at drastically different temperatures and line-broadening at higher temperatures could result in uncertainties of comparable magnitude in the measurements.

Energy level of the luminescence emitting state. From the luminescence data in Figure 7, the energy level of the emitting state in the U(VI) complexes (ΔE) is calculated to be 20198, 20137 and 20026 cm^{-1} for the $UO_2(L^I)_2$, $UO_2(L^{II})_2$ and $UO_2(L^{III})_2$ complexes, respectively. These values are the origins, or zero-phonon-lines for the charge transfer vibronic transition associated with the symmetric stretching mode of uranyl in the three complexes. As shown by the energy diagram in Figure 8 for the free uranyl cation (UO_2^{2+}), the value of ΔE corresponds to the gap between the HOMO (the $3\sigma_u$ orbitals mainly from oxygen) and LUMO (the δ_u and ϕ_u orbitals from uranium).[30,31] In complexes, the energy levels of uranyl vary as a function of ligand coordination *via* the equatorial plane. In most cases, the energy level of the LUMO is reduced, and so is the energy gap for the charge transfer transition. The stronger the ligand is, the smaller the gap could become. The values of ΔE from this work suggest that, among the three ligands under study, L^{III} (ODA) is the strongest and L^I (TMOGA) is the weakest, in agreement with the thermodynamic trend as well as all other structural and spectroscopic data from this work.
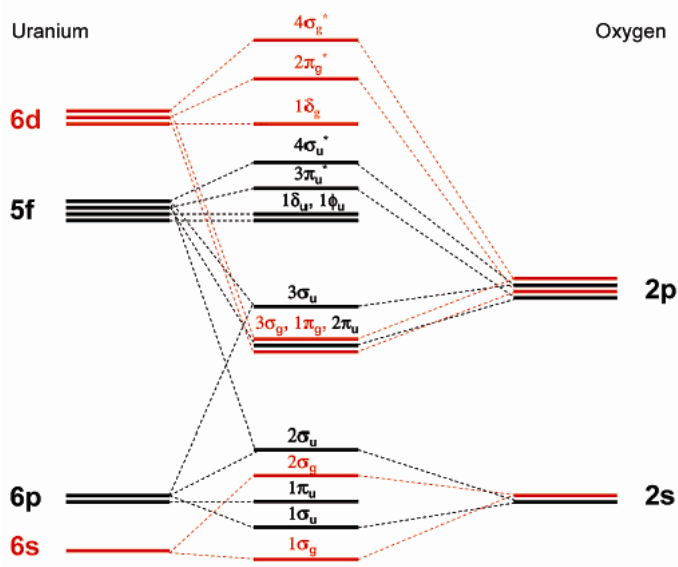

Figure 8. Schematic energy diagram of UO_2^{2+} valence orbitals.[30]

4. Conclusion

N, N, N′, N′-tetramethyl-3-oxa-glutaramide (TMOGA) and *N,N*-dimethyl-3-oxa-glutaramic acid (DMOGA) form tridentate complexes with U(VI) in a similar manner to oxydiacetic acid (ODA). Substitution of a carboxylate group with an amide group in the series of ODA-DMOGA-TMOGA makes the enthalpy of complexation more favorable (less endothermic) to the formation of complexes. However, the binding strength of the ligands for U(VI) decreases from ODA to DMOGA and further to TMOGA, mainly due to the decrease in the entropy of complexation along the series. With the structural and spectroscopic data obtained by a number of techniques, very good correlations between the thermodynamic properties and structural parameters (bond length, vibration frequency and the energy level of luminescence emitting state) have been established.

Though the oxa-diamides appear to be weaker ligands than their carboxylate analogs in aqueous solutions, they could still be highly effective extractants in solvent extraction because the great ease of attaching alkyl (or aryl) groups to the amide group(s) makes them readily soluble in many organic solvents. Besides, structural information on the U(VI)/TMOGA and U(VI)/DMOGA complexes suggest that the binding strength of oxa-diamides with actinides could be improved by increasing the entropy of complexation through rational design of ligands. For example, a ligand can be made by connecting two TMOGA molecules with proper alkyl "backbone" so that all the six oxygen atoms are in the optimal positions to coordinate UO_2^{2+} and other dioxo actinyl cations (e.g., NpO_2^+, NpO_2^{2+} and PuO_2^{2+}). The 1:1 complex of actinyl cations with such hexa-dentate oxa-amides (ML) should be much stronger than the 1:2 complex with the tridentate oxa-amides (ML$_2$) because of a larger entropy effect, as well as lower pre-organization energy for the hexa-dentate ligands.

Supporting Information: Three CIF files for structures of $UO_2(\mathbf{L^I})_2(ClO_4)_2$, $UO_2(\mathbf{L^{II}})_2(H_2O)(NaClO_4)_2$ and $Na_2UO_2(\mathbf{L^{III}})_2(H_2O)$.

REFERENCES

1. Suzuki, H.; Sasaki, Y.; Sugo, Y.; Apichaibukol, A.; Kimura, T. *Radiochim. Acta*, **2004**, *92*, 463–466.

2. Ansari, S. A.; Pathak, P. N.; Husain, M.; Prasad, A. K.; Parmar, V. S.; Manchanda, V.K. *Radiochim. Acta*. **2006,** 94, 307-312

3. Tian G.; Zhang P.; Wang J.; Rao L. *Solv. Extr. Ion Exch*. **2005**, *23* (5), 631-643.

4. Sasaki, Y.; Choppin, G. *Radiochim. Acta,* **1998**, *80*, 85–88.

5. Nave, S.; Modolo, G.; Madic, C.; Testard, F. *Solv. Extr. Ion Exch*. **2004**, *22* (4), 527–551.

6. Narita, H.; Yaita, T.i; Tachimori, S. *Solv. Extr. Ion Exch*. **2004**, *22* (2), 135–145.

7. Shimada, A.; Yaita, T.; Narita, H.; Tachimori, S.; Okuno, K. *Solv. Extr. Ion Exch*. **2004**, *22*(2), 147–161.

8. Sasaki, Y.; Sugo Y.; Tachimori, S. *Solv. Extr. Ion Exch*. **2001**, *19*(1), 91-103.

9. Tian, G.; Wang, J.; Song, C. *J. Nucl. Radiochem*. (Chinese), **2001**, *23*(3), 135-140.

10. Rao, L.; Tian, G., in "Recent Advances in Actinide Science", R. Alvarez, N. D. Bryan and I. May, eds., the Proceedings of the eighth Actinide Conference, Actinide 2005, Manchester, UK, July 4-8, 2005, RSC Publishing, 2006, pp.509-511.

11. Rao, L.; Tian, G., in *Actinides 2005 -- Basic Science, Applications and Technology*, J. L. Sarrao, A. J. Schwartz, M. R. Antonio, P. C. Burns, R. G. Haire, and H. Nitsche, Eds., (Mater. Res. Soc. Symp. Proc. 893, Warrendale, PA, 2006), Paper # 0893-JJ08-06.

12. Sugo, Y.; Sasaki, Y.; Tachimori, S. *Radiochim. Acta*, **2002**, *90*, 161-165.

13. Sill, C.; Peterson, H. E. *Anal. Chem.* **1947**, *19*, 646-651.

14. Gran, G. *Analyst*, **1952**, *77*, 661.

15. Rao, L.; Garnov, A. Y.; Jiang, J.; Bernardo, P. D.; Zanonato, P.; Bismondo, A. *Inorg. Chem.* **2003**, *42*, 3685-3692.

16. Gans, P.; Sabatini, A.; Vacca, A., Hyperquad 2000, v.2.0 (2000).

17. Zanonato, P.; Bernardo, P. D.;Bismondo, A.;Liu, G.; Chen, X.; Rao, L. *J. Am. Chem. Soc.* **2004**, *126*, 5515-5522.

18. Arnek, R. *Ark Kemi*. **1970**, *32*, 81.

19. SHELXTL, Bruker AXS, Madison, WI, USA.

20. Ressler, T. J. *Synch. Rad.*, 1998, *5*, 118.

21. Ankudinov, A. L.; Ravel, B.; Rehr, J. J.; Conradson, S. D. *Phys. Rev*. **1998**, *B 58*, 7565.

22. Martell, A. E.; Smith, R. M.; Motekaitis, R. J. NIST Critically Selected Stability Constants of Metal Complexes Data Base. NIST Stand. Ref. Database 46, U.S. Department of Commerce, Gaithersburg, MD, 1998.

23. Rao, L.; Tian, G. *J. Chem. Thermodynamics*, **2008**, 40, 1001-1006.

24. Grenthe, I.; Fuger, J.; Konings, R. J. M.; Lemire, R. J.; Muller, A. B.; Nguyen-Trung, C.; Wanner, H. "*Chemical thermodynamics of uranium*", (Wanner, H., Forest, I., eds.), Amsterdam: Elsevier Science Publishers B.V., 1992, p.268.

25. Jiang, J.; Sarsfield, M. J.; Renshaw, J. C.; Livens, F. R.; Collison, D.; Charnock, J. M.; Helliwell, M.; Eccles, H. *Inorg. Chem*. **2002**, 41, 2799–2806.

26. Nguyen-Trung, C.; Begun, G. M.; Palmer, D. A. *Inorg. Chem.* **1992**, 31, 5280-5287.

27. Jones, L. H.; Penneman, R. A. *J. Chem. Phys*. **1953**, 21, 542-544.

28. Metcalf, D. H.; Dai, S.; Del Cul, G. D.; Toth, L. M. *Inorg. Chem*. **1995**, 34, 5573.

29. Liu, G. K.; Chen, X. Y.; Huang, J. *Mol. Phys*. **2003**, 101, 1029.

30. Denning, R. G. *J. Phys. Chem*. A **2007**, 111, 4125-4143.

31. Liu, G. K.; Beitz, J. V., in *The Chemsitry of the Actinide and Transactinide Elements*, ed. L. R. Morss, N. M. Edelstein and J. Fuger, Springer, Dordrecht, 3rd edn, 2006, Vol. 3, p. 2087.

Graphical Abstract

Absorption spectra of U(V) complexes with ODA, DMOGA and TMOGA ligands